Resonant Frequency Analysis using Perturbation and Resonant Cavity Method in Printed Dual Band Antenna for WiMAX Application

C. Mahendran[1] and M. Vijayaraj[2]

[1]Department of Electronics and Communication Engineering
Alagappa Chettiar Government College of Engineering and Technology, Karaikudi-630003, Tamilnadu, India
mahendrangc@gmail.com

[2]Department of Electronics and Communication Engineering
Government College of Engineering, Tirunelveli-627007, Tamilnadu, India
mvijayaraj25567@gmail.com

Abstract – A printed dual-band antenna is designed to resonate at 3.5 GHz with the measured gain of 6.38 dBi and at 5.5 GHz with that of 5.84 dBi for the WiMAX application. The bandwidth of this antenna at 3.5 GHz and 5.5 GHz is 8% and 5%, respectively. The radiation efficiency of 91.45% is obtained at 3.5 GHz and that of 89.56% at 5.5 GHz. A novel approach based on the perturbation technique is used to relate the resonant frequency to the electromagnetic energy stored and the volume of the proposed antenna's structure. The dual resonant length of this antenna is determined by a parameter named as the length reduction factor, which is computed by the curve fitting method. A polynomial equation connects the length reduction factor and resonance frequency. The resonant cavity model has been used to derive the resonant frequency equations for dual bands. The simulation and measured results are used to validate the analytically predicted resonant frequency caused by the structure perturbation and cavity technique and show good agreement. This antenna is fed by a balanced parallel plane, which conveniently facilitates the PCB's integration.

Index Terms – curve fitting, electric and magnetic energy, perturbation technique, polynomial equation, printed antenna, resonant cavity, WiMAX band.

I. INTRODUCTION

Around the world, every domestic and official activity has been computerized. As a result, high-speed internet access in emerging countries' rural areas is required. Orthogonal Frequency Division Multiplexing (OFDM) can be incorporated into WiMAX to provide a higher data rate without selective fading. A printed or microstrip antenna is the ideal tool for transmitting and receiving the WiMAX band of frequencies. It is affordable, lightweight, and takes up less space on mobile phones, laptops, and other electronic devices.

Numerous antennas for the WiMAX band that operate at 3.5 GHz and 5.5 GHz have been documented in the literature. These types include printed monopoles, ring-shaped patches, defective ground plane antennas, metamaterial loaded antennas, and MIMO antennas, according to Refs. [1–15]. In addition, coplanar waveguide-fed microstrips, Minkowski-Sierpinski carpet fractal constructed, complementary split-ring resonator-based, meander line slotted antennas, and Vicsek Fractal slotted antennas are reported in [16–26].

In order for a WiMAX signal to traverse a great distance, the antenna gain is critical. The gain of these reported antennas is lower. The antennas listed in the literature have either a full or partial ground plane, and most of them employ a microstrip line as a feeder, which necessitates the ground plane. Because the RF currents are carried via the pair of tracks on the printed circuit board (PCB), it is difficult to integrate the antenna with microwave or RF printed circuitry. This challenge is a result of the ground plane being a part of the antenna structure. The feeder lines in these reported antennas are unbalanced, although the tracks on the PCB are balanced. Consequently, compatibility issues exist between these antennas and the PCBs of high-frequency circuitry.

A novel mitigation strategy is proposed in this article to address these issues. A printed antenna is designed to radiate in the WiMAX band (3.5 GHz and 5.5 GHz) with a balanced line feeder. This proposed antenna does not require any full or partial ground plane as a part of the feeding structure, which facilitates the uniform field distribution. As a result, it is self-shielding to some extent. As it has a balanced line feeder, integrating this proposed printed antenna with the PCB of RF circuitry is very compatible. The gain of this proposed antenna is much better than that of those antennas reported in

Submitted On: August 24, 2022
Accepted On: January 23, 2023

https://doi.org/10.13052/2023.ACES.J.380206

the literature. The analytical expression for the resonant frequency of this proposed antenna is derived with the aid of perturbation and the resonant cavity method. This theoretical concept of perturbation is applied to the permittivity measurement of polystyrene mixed with carbon black fillers [27], and the computation of resonant frequency in a rectangular dielectric resonator antenna [28].

II. ANTENNA DESIGN

The dimensions of the proposed dual-band printed antenna are 48.5 mm × 97 mm × 1.6 mm. The RT Duroid 5880 substrate was used to make this antenna, which has a relative permittivity of 2.2. A pair of balanced copper strip lines are printed to feed RF current into the radiating patch, with the appropriate length (Lf) and width (Wf) determined by the CST Studio Suite simulator to deliver the optimum signal level to the patch over the WiMAX band of frequency range.

This balanced line ensures a consistent electric field distribution between the strips. This mechanism ensures self-shielding, which reduces the undesired radiation from the feeder line. The proposed antenna's top and bottom views are depicted in Fig. 1, and its dimensions are provided in Table 1. To move the resonance from lower to higher frequency, the right-hand side edge of the top patch and the corresponding region on the bottom side are perturbed in this antenna. The unperturbed antenna resonates at a lower frequency. Resonant cavity modelling is used to calculate the length (Lr1, Lr2) and width (Wr) of the patch and ground plane. The width (Wx) is stretched along the Y-axis, whose dimension is determined by CST Studio Suite simulation, in order to enhance the gain.

Table 1: Dimensions of antenna

Parameter	Lf	Wf	Lr1	Lr2	Wr	Wx
Dimension (mm)	9	26	15.5	24	63	17

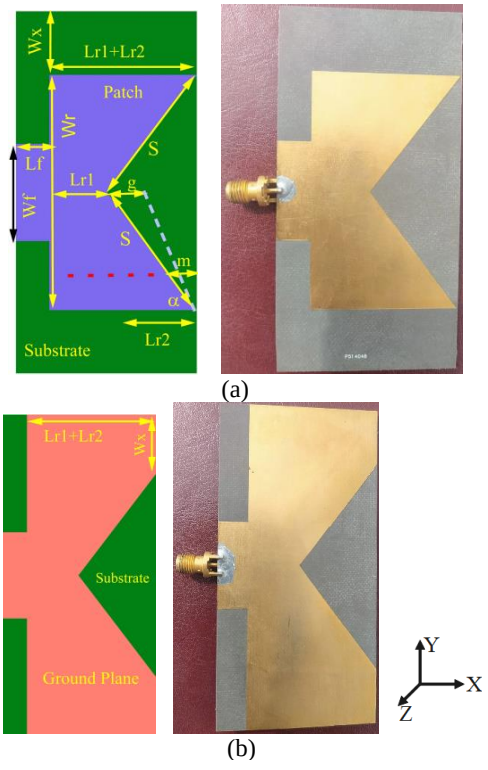

Fig. 1. Perturbed antenna. (a) Top view. (b) Bottom view. m = m1 at 3.5 GHz. m = m2 at 5.5 GHz.

III. RESONANT FREQUENCY ANALYSIS

The resonant frequency of this proposed antenna is analyzed using the cavity model and perturbation technique. With CST simulation and measurement using Vector Network Analyzer, the expected resonant frequency derived from these two analytical techniques is validated. All these results are matched well, ensuring the accuracy of the analytical procedure.

IV. RESONANT CAVITY METHOD

This proposed antenna forms a cavity filled with RT Duroid 5880 dielectric of a thickness (h) bounded by (Lr1+Lr2) × Wr × h mm^3. This resonant cavity supports two distinct resonant lengths, 3.5 GHz along Y-axis and 5.5 GHz along X-axis, as shown in Fig. 1 (a), causing a dual band of radiation. As there is no tapering along the Y-axis, the resonant length along this axis is constant, whereas the resonant length along the X-axis is variable due to tapering. The expression for the resonant frequency of these two bands is described in the following sections.

A. WiMAX band of 3.5 GHz

Equation (1) states that for an antenna to resonant at 3.5 GHz, the resonant length along the Y-axis connecting the radiating slots should be one half of the guide wavelength (λ_1) at 3.5 GHz:

$$Wr + 2h = 0.5\lambda_1, \tag{1}$$

where electric field fringing at both ends along Y-axis is incorporated as '2h'. This fringing field should be taken into account due to the ground plane extension in the bottom side of antenna. For microstrip or printed antenna design, the resonant length extension can be approximated by $\frac{h}{\sqrt{\varepsilon_1}}$ for one radiating edge [29]. Here it is taken as 'h' approximately against the actual computed value of 0.7h. 'λ_1' can be computed from Eqn. (1) as follows:

$$\lambda_1 = 132.4\ mm. \tag{2}$$

The length along the X-axis connecting the non-radiating slots is not constant due to the presence of

tapering and is represented by Eqn. (3). The effective length will be less than 'Lr2', which is represented by 'Lr2-m1', where 'm1' is length reduction factor. The value of 'm1' is 6.4mm, which is computed from MATLAB program:

$$Lr1 + Lr2 - m1 = 33.1\ mm = 0.3\lambda_1. \quad (3)$$

As there is no conductive plane extension at the ground plane, fringing field is neglected at both left and right edge of patch, compared to top and bottom edge.

Equation (4) represents the resonant frequency (f_1) corresponds to 3.5 GHz band [30]:

$$f_1 = \frac{150}{\sqrt{\varepsilon_1}}\sqrt{\left(\frac{P}{Lr1 + Lr2 - m1}\right)^2 + \left(\frac{Q}{Wr + 2h}\right)^2} \quad (4)$$
$$GHz = 3.497\ GHz,$$

where Lr1, Lr2, m1, Wr and h are in 'mm'.

'P' is an integer represents the half-cycle electric field variation along the X-axis and Q for Y-axis. For 3.5 GHz, P=1 and Q=1 from Eqn. (3) and Eqn. (1), respectively. As the 'P' has to be an integer to satisfy the boundary condition requirements, the nearest integer unity has been taken to satisfy the Eqn. (3). As the thickness 'h' is very small, the field variation along the Z-axis is negligible. The effective permittivity 'ε_1' is given by Eqn. (5) [30]:

$$\varepsilon_1 = \frac{\varepsilon_r + 1}{2} + \frac{\varepsilon_r - 1}{2}\left[1 + 12\frac{h}{W}\right]^{-0.5} = 2.1. \quad (5)$$
$$W = W1 = Lr1 + Lr2 - m1 \text{ at 3.5 GHz}$$
$$W = W2 = Wr + 2h \text{ at 5.5 GHz}$$

The mode of operation at 3.5 GHz is Transverse Magnetic to Z-axis ($TM^Z{}_{110}$).

B. WiMAX band of 5.5 GHz

The resonant length condition for 5.5 GHz band is given in Eqn. (6):

$$Lr1 + Lr2 - m2 = 0.5\ \lambda_2. \quad (6)$$

The length reduction factor 'm2' for this band is 16.9 mm, calculated from the MATLAB program. Equation (7) depicts the guide wavelength at 5.5 GHz.

$$\lambda_2 = 45.2\ mm. \quad (7)$$

The length which connects the non-radiating slots of this 5.5 GHz band is represented by the Eqn. (8):

$$Wr = 63\ mm = 1.39\ \lambda_2. \quad (8)$$

The nearest integers that satisfy the boundary condition of the cavity model are 'P' = 1 and 'Q' = 2. If 'Q' = 3 refers to the mode integer along the length linking the non-radiating slots, the length reduction factor 'm2' in the MATLAB program turns negative, ruling out the solution. The negative value of 'm2' refers to the length extension rather than the intended reduction. To make the 'm2' positive, the mode integer 'P' has to be increased, which does not mean full. 'P' should be '1' because it refers to the half-cycle field variation along the resonant length. Moreover, the length extension of '2h' due to the fringing field is insignificant for the non-radiating side of the patch as it regulates the impedance matching only at the band of interest. Hence 'Wr' is the most significant term for the integer value computation for 'Q' in Eqn. (8). The resonant frequency (f_2) expression for 5.5 GHz band is given by Eqn. (9):

$$f_2 = \frac{150}{\sqrt{\varepsilon_2}}\sqrt{\left(\frac{P}{Lr1 + Lr2 - m2}\right)^2 + \left(\frac{Q}{Wr}\right)^2} \quad (9)$$
$$GHz = 5.58 GHz.$$

Equation (5) with the appropriate 'W' value is used to calculate the effective permittivity 'ε_2'. The calculated value is 2.13, and the mode of operation is $TM^Z{}_{120}$.

C. Length reduction factor computation

The length reduction factor plays a more vital role in the 5.5 GHz resonant band than in the 3.5 GHz band, as it appears in the resonant length expression of 5.5 GHz. The length along the X-axis varies almost linearly due to tapering. Therefore, numerous resonance lengths are feasible. One of these variable lengths has been set (activated) for 5.5 GHz resonance by matching the port impedance with the resonator exclusively for the 3.5 and 5.5 GHz bands, as depicted in Fig. 1 (a) as a red dashed line. Whereas, all other frequencies are not matched, hence those other resonant frequencies are not set. This is demonstrated in Figs. 8 (a), (b) and Figs. 6 (c) through (f). Therefore, 'm' specifies the length reduction necessary to activate the specified band. A MATLAB program is written to predict the 'm1' value for the 3.5 GHz band and the 'm2' value for the 5.5 GHz band. Angle 'α' can be varied by varying the parameter 'g' as shown in Fig. 1 (a), which alters the length of 'Lr2' to 'Lr3' as given by Eqn. (10):

$$Lr3 = Lr2 - g. \quad (10)$$

The 'α'and 'Lr3' can be related by the Eqns. (11a) or (11b):

$$\alpha = \tan^{-1}\left[\frac{Wr/2}{Lr3}\right] radian, \quad (11a)$$

$$\alpha = \frac{180}{\pi}\tan^{-1}\left[\frac{Wr/2}{Lr3}\right] degree. \quad (11b)$$

The 'm1' or 'm2' value also varied accordingly, influencing the resonant frequency in the 3.5 GHz or 5.5 GHz band. The resonant frequencies are noted from the simulator for each 'α' or 'g' value. The 'm1' or 'm2'

value depends on the effective electrical length along the X-axis. This is an unknown parameter. This 'm1' or 'm2' is predicted using the MATLAB program, whose algorithm is listed below:

Step 1: Keep all the parameters are constant except 'f_1' ('f_2') and 'm1' ('m2') in Eqn. (4) (Eqn. (9)) for the 3.5 GHz (5.5 GHz) band.

Step 2: Vary the 'α' or 'g' values and note the resonant frequency in the CST Studio Suite simulator. Feed these simulated resonant frequencies 'f_1s' ('f_2s') into MATLAB program.

Step 3: Arbitrarily vary the 'm1' ('m2') value with the step size of 0.001 mm and calculate the resonant frequency as 'f_1m' ('f_2m') using MATLAB coding.

Step 4: Store the 'm1' ('m2') values when the deviation between 'f_1m' ('f_2m') and 'f_1s' ('f_2s') is less than 0.0001 GHz.

The expressions that relate the 'm1' ('m2') values with 'f_1' ('f_2') are derived with the aid of curve fitting technique in MATLAB.

For 3.5 GHz Band, 3.044 GHz $\leq f_1 \leq$ 3.5 GHz,

$$m1 = -234.5{f_1}^{-1.904} + 28.03, \quad (12)$$

$$m1 = -6.425{f_1}^{2} + 56.42f_1 - 112.3. \quad (13)$$

For 5.5 GHz Band, 4.568GHz $\leq f_2 \leq$ 5.51 GHz,

$$m2 = -1503{f_2}^{-2.861} + 28.31, \quad (14)$$

$$m2 = 1.324{f_2}^{3} - 23.32{f_2}^{2} + 142.5f_2 - 281.5. \quad (15)$$

Equation (12) and Eqn. (14) represent the general power2 model. The linear polynomial of degree 2 and 3 models are represented by Eqn. (13) and Eqn. (15), respectively. Among these models, the general power2 model relates the 'm1' ('m2') with 'f_1' ('f_2') better than the linear polynomial of degree 2 or degree 3 model. The R-square value is 1 for both models, which ensures the best goodness of fit. Figure 2 depicts this relationship. As the patch is perturbed, the resonant frequency is shifted from a lower to a higher value as shown in Fig. 3.

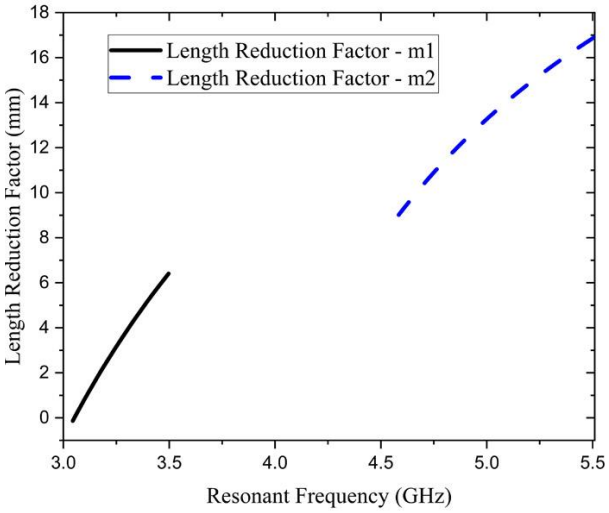

Fig. 2. Length reduction factor.

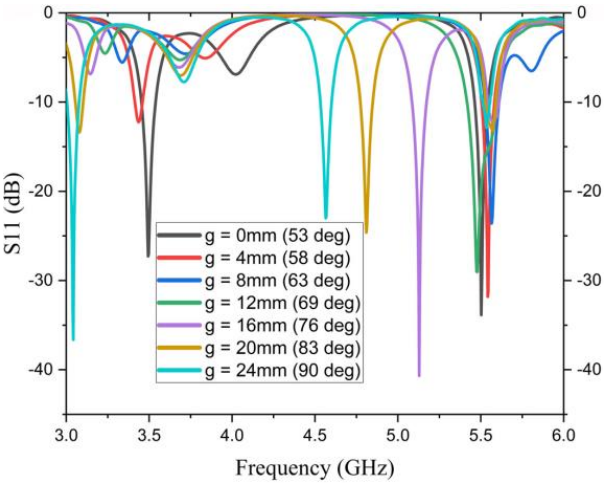

Fig. 3. Resonant frequency shifts due to perturbation.

V. PERTURBATION TECHNIQUE

The solution of the homogeneous wave equation in terms of vector potential (Az) for this proposed antenna has been obtained using the differential equation method (separation of variables). Then the fields and the expression for resonant frequency are derived from 'Az'. This approach leads to an exact solution for this antenna that resembles an RT Duroid dielectric-loaded resonant cavity. However, many electromagnetic field problems such as microwave resonators, waveguides and antenna problems cannot be solved using the conventional differential equation method due to the mathematical complexity involved in the structural definition and boundary conditions. The perturbational method is an alternative approach for solving electromagnetic problems, including antenna analysis. The word 'perturb' means to disturb or to change slightly. The perturbational method is useful for calculating the shift in resonant frequency due to changes in the structure of the printed antenna. Two kinds of structures involved in this proposed printed antenna. One kind is the 'unperturbed' structure, for which the resonant frequency is known (3.04 GHz at 3.5 GHz band and 4.57 GHz at 5.5 GHz band), and the other is the 'perturbed' structure, which is different from the unperturbed one. The perturbed and unperturbed printed antennas are shown in Fig. 1 and Fig. 4, respectively. The electromagnetic energy is stored in the volume of 3981.6 mm^3 in the unperturbed antenna, bounded by

(Lr1+Lr2) × Wr × h mm^3. The right-hand side edge of the antenna is perturbed in both patch and ground plane, which reduces the conducting surface area in that region, which in turn removes the volume of 1209.6 mm^3.

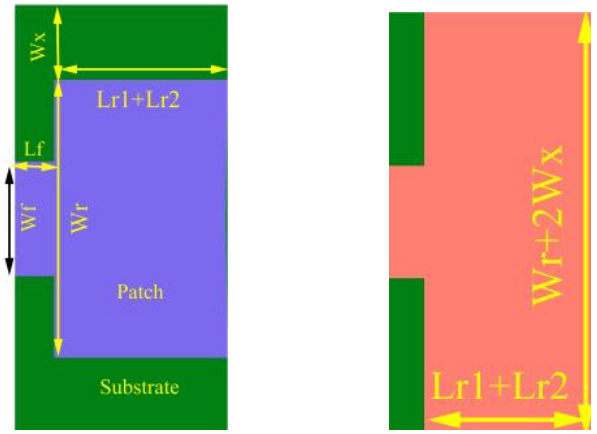

(a) (b)

Fig. 4. Unperturbed antenna. (a) Top view. (b) Bottom view.

Consequently, the stored energy is also removed in that volume governed by the removed surface area and the thickness of the substrate. Equation (16) relates the resonant frequency shift with the volume and energy stored in the resonant cavity [31]:

$$\frac{f_i - f_{0i}}{f_{0i}} = a_i = \frac{V_\alpha}{V} = \frac{W_{i\alpha}}{W_i}, \tag{16}$$

where, 'f_i' is the shifted resonant frequency due to perturbation or resonant frequency of the perturbed antenna. 'f_{oi}' is the resonant frequency of the unperturbed antenna. 'a_i' is the parameter that depends on the antenna structure and the position of the perturbation. 'V_α' is the removed volume due to perturbation. 'V' is the volume of the unperturbed antenna. '$W_{i\alpha}$' is the removed energy due to perturbation or stored energy in the volume defined by the product of removed patch area and thickness of the antenna. 'W_i' is the stored energy in the volume defined by the unperturbed antenna:

i = 1 for 3.5 GHz band

i = 2 for 5.5 GHz band

A change in the input power to the antenna will not affect the estimated frequency since the resonant frequency shift is proportional to the change in stored energy relative to the total energy stored in the unperturbed resonant cavity. For various input power levels, the stored and removed energy level will be proportionally varied. Consequently, the energy ratio will remain constant.

A. WiMAX 3.5 GHz band

The resonant frequency of the unperturbed antenna 'f_{o1}' is 3.04 GHz from Eqn. (4) with the effective value of 'm1' equals −0.133. The physical value of 'm1' equals zero also predicts the resonant frequency of the unperturbed antenna as 3.05 GHz, which is very close to 3.04 GHz. CST Studio Suite simulation demonstrating 3.04 GHz validates the calculated result. When it is perturbed at the right-hand edge, the frequency has shifted to 3.5 GHz. More perturbation is taking place at the position where its magnetic field is maximum.

The resonant frequency shift 'f_1' caused by perturbation in the antenna's structure can be computed using Eqn. (16):

$$V = (Lr1 + Lr2) \times Wr \times h = 3981.6\ mm^3, \tag{17}$$

$$V\alpha = 0.5 \times Lr2 \times Wr \times h = 1209.6\ mm^3. \tag{18}$$

The electric and magnetic field expressions within the antenna structure (taken as cavity resonator) are given by Eqn. (19) to Eqn. (24) [30]:

$$\mathrm{E_x} = \frac{-\mathrm{jK_zK_x}}{\omega\mu\varepsilon} A_{pqr} \operatorname{Sin}(\mathrm{K_x x}) \operatorname{Cos}(\mathrm{K_y y}) \operatorname{Sin}(\mathrm{K_z z}), \tag{19}$$

$$\mathrm{E_y} = \frac{-\mathrm{jK_zK_y}}{\omega\mu\varepsilon} A_{pqr} \operatorname{Cos}(\mathrm{K_x} x) \operatorname{Sin}(\mathrm{K_y y}) \operatorname{Sin}(\mathrm{K_z z}), \tag{20}$$

$$\mathrm{E_z} = \frac{-\mathrm{j}(k_i^2 - K_z^2)}{\omega\mu\varepsilon} A_{pqr} \operatorname{Cos}(\mathrm{K_x} x) \operatorname{Cos}(\mathrm{K_y y}) \operatorname{Cos}(\mathrm{K_z z}), \tag{21}$$

$$\mathrm{H}_x = \frac{K_y}{\mu} A_{pqr} \operatorname{Cos}(\mathrm{K_x} x) \operatorname{Sin}(\mathrm{K_y y}) \operatorname{Cos}(\mathrm{K_z z}), \tag{22}$$

$$\mathrm{H}_y = \frac{-K_x}{\mu} A_{pqr} \operatorname{Sin}(\mathrm{K_x} x) \operatorname{Cos}(\mathrm{K_y y}) \operatorname{Cos}(\mathrm{K_z z}), \tag{23}$$

$$H_z = 0. \tag{24}$$

All of the above equations contain the mode-dependent amplitude coefficient 'Apqr', which scales the amplitude of all fields equally. As only TM$^z_{110}$ mode exists in this 3.5 GHz band, the 'Apqr' value will be the same for all fields. Therefore, its value is taken as unity. Moreover, all fields can be normalized by this coefficient to make its presence insignificant. The wavenumbers are expressed by the Eqn. (25) to Eqn. (28):

$$K_x = \frac{p\pi}{Lr1 + Lr2 - m1} = 95, \tag{25}$$

$$K_y = \frac{q\pi}{Wr + 2h} = 47.46, \tag{26}$$

$$K_z = \frac{r\pi}{h} = 0, \tag{27}$$

$$k_i = k_1 = \omega_1 \sqrt{\mu\varepsilon_1}. \tag{28}$$

The field variation along the Z-axis is negligible because the antenna's thickness is minimal to its operating wavelength. The denominator of Eqn. (25) determines the resonant length. The stored energy is computed for the band of interest, such as 3.5 and 5.5 GHz. Hence, the resonant length is the effective length along the X-axis, which is considered for stored energy calculation. The total energy stored in the electric field 'W_{e1}' and

magnetic field 'W_{m1}' at 3.5 GHz of an unperturbed antenna of volume 'V' is given by Eqn. (29) to Eqn. (32):

$$W_{e1} = \frac{\varepsilon_1}{2}\iiint |E_z|^2 dv = 4.947KJ, \tag{29}$$

with the integral limit for Eqn. (29), Eqn. (31) and Eqn. (32): x = 0 to Lr1+Lr2; y = 0 to Wr and z = 0 to h:

$$W_{m1} = W_{Hx} + W_{Hy} = 4.875KJ, \tag{30}$$

$$W_{Hx} = \frac{\mu}{2}\iiint |H_x|^2 dv = 1.054KJ, \tag{31}$$

$$W_{Hy} = \frac{\mu}{2}\iiint |H_y|^2 dv = 3.821KJ. \tag{32}$$

The energy stored in the electric and magnetic fields is almost the same at resonance. The perturbation technique is applied to predict the resonant frequency shift for two cases of energy perturbation.

Case 1: Electric energy perturbation

The part of the electric energy '$W_{1\alpha e}$' removed by the volume 'Vα' due to perturbation from the total stored energy is 1503 J. The ratio of removed energy to total stored energy in the electric field is given by the Eqn. (33):

$$\frac{W_{1\alpha e}}{W_1} = \frac{1503J}{2W_{e1}} = 0.153. \tag{33}$$

The shifted resonant frequency and parameter 'a1e' is predicted using the Eqn. (16) that relates the energy and volume ratio with the frequency ratio given by Eqn. (34) and Eqn. (35):

$$f_{1e} = 1.153 f_{01} = 3.505GHz, \tag{34}$$

$$a_{1e} = 0.5036. \tag{35}$$

Case 2: Magnetic energy perturbation

Magnetic energy of 1481J is removed by 'Vα' in this case. The magnetic energy ratio is given by Eqn. (36):

$$\frac{W_{1\alpha m}}{W_1} = \frac{1481J}{2W_{m1}} = 0.152. \tag{36}$$

The shift in resonant frequency and parameter 'a1m' is given by Eqn. (37) and Eqn. (38)

$$f_{1m1} = 1.152 f_{01} = 3.502GHz, \tag{37}$$

$$a_{1m1} = 0.5. \tag{38}$$

If 'W1' is the summation of energy stored in the electric and magnetic fields at the resonance, then Eqn. (39) and Eqn. (40) will result.

$$f_{1m2} = 1.151 f_{01} = 3.499GHz, \tag{39}$$

$$a_{1m2} = 0.497. \tag{40}$$

The same result is estimated for the resonant frequency shift resulting from perturbation from both electric and magnetic energy perturbation cases and is confirmed by simulation and measurement.

B. WiMAX 5.5 GHz band

The resonant length in 3.5 GHz band is the length connecting the lower edge 'AB' to upper edge 'ED' as illustrated in Fig. (5) and is uniform. Whereas for 5.5 GHz band, the length connecting the left edge 'AE' to right edge 'BCD' is the resonant length and is not uniform due to the presence of perturbation. The 'm2' value corresponds to the effective length responsible for 5.5 GHz resonance is calculated using MATLAB program and simulation. The unperturbed antenna structure resonates at 4.57 GHz in the simulation, whereas, the Eqn. (9) predicts the resonance at 4.1 GHz. The simulated resonant frequency of 4.57 GHz is taken as the resonant frequency of the unperturbed antenna. For this 5.5 GHz band, the same procedure is followed as in section V. A for 3.5 GHz band to compute the resonant frequency shift using perturbation technique, and the results are furnished below:

Equation (41) to Eqn. (44) express the wavenumbers:

$$K_x = \frac{p\pi}{Lr1 + Lr2 - m2} = 139, \tag{41}$$

$$K_y = \frac{q\pi}{W_r} = 99.73, \tag{42}$$

$$K_z = \frac{r\pi}{h} = 0, \tag{43}$$

$$k_i = k_2 = \omega_2\sqrt{\mu\varepsilon_2}. \tag{44}$$

The field variation along the Z-axis is negligible because of the thin substrate compared to the operating wavelength. The total energy stored in the electric field ' W_{e2}' at 5.5 GHz of an unperturbed antenna of volume 'V' is expressed by Eqn. (45):

$$W_{e2} = \frac{\varepsilon_2}{2}\iiint |E_z|^2 dv = 10.187KJ, \tag{45}$$

with the integral limit for Eqn. (45): x = 0 to Lr1+Lr2; y = 0 to Wr and z = 0 to h. As the energy stored in the electric field will be the same as that in magnetic fields at resonance, the total energy stored in the antenna structure will be twice the energy stored in the E-field. This stored electric energy calculation is enough to predict the resonant frequency shift due to perturbation using the perturbation technique. Therefore, the energy stored in the H-field calculation is not necessary.

The part of the electric energy '$W_{2\alpha}$' of 3.1KJ is removed by the volume 'Vα' due to perturbation from the total stored energy. The ratio of removed energy to total stored energy in the electric field is illustrated by Eqn. (46):

$$\frac{W_{2\alpha}}{W_2} = \frac{3.1KJ}{2W_{e2}} = 0.152. \tag{46}$$

The shifted resonant frequency 'f_{2ea}' and parameter 'a2ea' are predicted analytically using Eqn. (16) as illustrated by Eqn. (47) and Eqn. (48).

$$f_{2ea} = 1.152 f_{02} = 5.3GHz, \tag{47}$$

$$a_{2ea} = 0.5. \tag{48}$$

The ratio of the resonant frequency of a perturbed (f_{2s}) to an unperturbed (f_{02}) antenna from the simulation

is given by Eqn. (49):

$$\frac{f_{2s}}{f_{02}} = \frac{5.5GHz}{4.57GHz} = 1.2. \quad (49)$$

The ratio of the removed energy '$W_{2\alpha s}$' to total energy 'W_{2s}' computed from Eqn. (16) corresponding to Eqn. (49) is illustrated by Eqn. (50):

$$\frac{W_{2\alpha s}}{W_{2s}} = 0.2. \quad (50)$$

The parameter 'a2s' corresponds to Eqn. (50) is calculated from Eqn. (16) and is given by Eqn. (51):

$$a_{2s} = 0.658. \quad (51)$$

The simulated resonant frequency shift due to perturbation is validated with the measured result using a vector network analyzer (ZNB20, Rohde & Schwarz) as shown in Fig. 8. Equation (52) depicts the deviation (d) between the measured frequency shift and that obtained from a calculation using the analytical method (resonant cavity method):

$$d = \left(\frac{f_{2s} - f_{2ea}}{f_{2s}}\right) \times 100 = 3.6\%. \quad (52)$$

It is observed from Eqn. (16) that the resonant frequency shift due to perturbation is determined by the energy removed in the perturbed volume. Equation (50) reveals that 20% of the total stored energy is removed due to perturbation, whereas Eqn. (46) predicts that 15.2% of that has been removed. A deviation of 4.8% exists between simulation and analytical computation based on the resonant cavity method. The removed energy predicted by the analytical method is lower than that of simulation, which eventually leads to the deviation in the resonant frequency shift, as notified by Eqn. (52). To validate this proposed perturbation technique, few antennas with slots and slits are selected from the literature [32–35]. In the aforementioned research, the shifted resonant frequencies are explored qualitatively rather than analytically. When the corners of a square patch are trimmed in Ref. [32], the patch's resonant frequency is shifted to 2.44 GHz from 2.4 GHz. The resonant frequency shift due to the addition of five slits on a radiating patch is reported in [33]. It is studied that the resonant frequency has shifted towards a higher value as the slits are added one by one from about 2.3 GHz to 7.5 GHz. Square-shaped slits and truncated corners are introduced on a patch fabricated using cotton and denim clothes as substrate [34]. The resonant frequency has shifted from 2.43 GHz to 2.53 GHz when the patch is perturbed. A square cavity formed by a substrate integrated waveguide, backed slot antenna is presented in [35]. An inward cut is made at the bottom right corner of the square cavity. As the size of the inward cut increases, the effective volume decreases. Eventually, the resonant frequency of the antenna increases. When these stated results are examined from the perspective of the perturbation approach, the energy removed from the volume corresponding to the region where the slits and truncations are taking place is what causes the resonant frequency shifting. In these described works [32–35], the eliminated energy causes the resonance to change from a lower to a higher value.

VI. RESULTS AND DISCUSSION

The proposed printed antenna has two resonant lengths, responsible for 3.5 GHz along the Y-axis and 5.5 GHz along the X-axis, as shown in Fig. 1. The surface current density plot illustrated in Figs. 6 (a) and 6 (b) ensures that the current flows between the top and bottom edges for 3.5 GHz resonance, and for 5.5 GHz, it flows between left and right edges. The E-field contour plot shown in Fig. 6 (c) demonstrates the electric field variation along the X and Y axes. There is a null between the maximum field that occurs at either end. This scenario ensures the TM^{Z}_{110} mode for 3.5 GHz resonance. In Fig. 6 (d), the horizontal white-coloured dashed line refers to the resonant path length responsible for the 5.5 GHz band. It is observed that a null occurs in between the two field maxima, and it refers to a one half-cycle variation along the X-axis. Three maximum field clusters with two nulls along the white-coloured vertical dotted line indicate the two half-cycle electric field variation along the Y-axis.

It dictates TM^{Z}_{120} mode at 5.5 GHz resonance. Figures 6 (e) and (f) show the magnetic field contour with the most significant amplitude corresponding to the space where the E-field is least and vice versa.

The resonant frequency of the unperturbed antenna is 3.04 GHz and 4.57 GHz, which has shifted to 3.5 GHz and 5.5 GHz, respectively, when its right-side edge is perturbed. This perturbation is made by removing copper on both the top and the corresponding bottom side.

However, the RT Duroid substrate is left in place, as illustrated in Fig. 1. When the copper and substrate of the perturbed volume are fully removed as shown in Fig. 5, little more energy is lost than in the perturbed structure, which eventually shifts the resonance further as depicted in Fig. 7. The simulated and measured return loss of the perturbed antenna is plotted in Fig. 8 (a), which shows the impedance bandwidth of 8% (3.35–3.64 GHz) at the 3.5.

GHz band and 5% (5.36–5.65 GHz) at the 5.5 GHz WiMAX band. Figure 8 (b) depicts the input reactance of the antenna, which ensures zero reactance at the resonant frequencies. Figures 9 and 10 depict the co and cross-polarization pattern at 3.5 GHz for E- and H-planes, respectively. This antenna is a broadside radiator, and the maximum radiation is taking place towards the normal to the patch. The cross-pol level is less than

−50 dB in E-plane at the maximum radiation direction and −120 dB in the H-plane. The polarization pattern at 5.5 GHz for both E and H-plane is shown in Figs. 11 and 12, respectively. It is observed that the cross-pol level is about −90 dB in the E-plane and −70 dB in the H-plane. A sharp null exists in the normal direction to the plane of the patch, and the main beam is tilted to 18° from the normal in the H-plane, which looks like a split beam. This split is due to the cut at the right edge of the perturbed antenna.

The simulated and measured gain are illustrated in Fig. 13. The simulated gain is 6.62 dBi at 3.5 GHz, whereas measured gain is 6.38 dBi. The simulated and measured gain for 5.5 GHz are 6.07dBi and 5.84 dBi, respectively. The measured gain at 5.5 GHz is less than that of 3.5 GHz due to the tapering at the right edge of perturbed antenna shown in Fig. 5. The red line shown in Fig. 5 is the resonant length for 5.5 GHz. A small amount of the electric field around this line at the left side (AE) forms the radiating slot. The electric field marked as 'E2' at the right side (BCD) has normal and tangential components. The angle between 'AB' and 'BC' is 53°. The angle between the electric field vector 'E2' and the edge 'AB' or 'ED' is 37°. The 'E2' vector is resolved into normal and tangential components expressed by Eqn. (53).

$$\overline{E_2} = \hat{x}E_2 Cos37^\circ \pm \hat{y}E_2 Sin37^\circ = 0.799E_2\hat{x} \pm 0.602E_2\hat{y}. \quad (53)$$

Sign is positive for taper line 'BC' and negative for taper line 'CD'. The tangential component '0.799E_2' is constructively added with the corresponding E-field at the side 'AE', whereas the normal component '0.602E_2' is destructively added between 'BC' and 'CD'. About 20% of 'E2' field is lost due to tapering at the right side of the patch. This field loss reduces the field strength in the radiating slot, and the gain is also lowered accordingly. As there is no tapering in the resonant length for 3.5 GHz, its gain is not suffered.

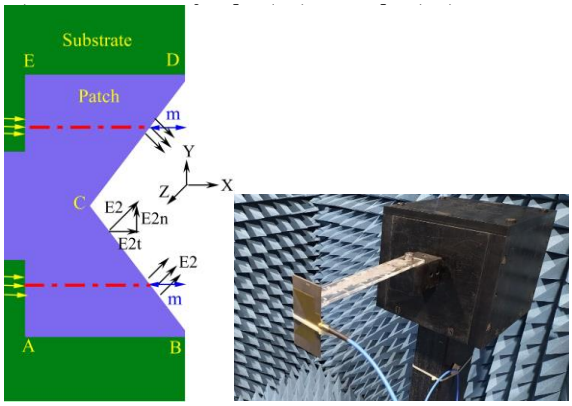

(a) (b)

Fig. 5. (a) Perturbed antenna with removed perturbed volume. m = m1 at 3.5 GHz. m = m2 at 5.5 GHz. (b) Antenna in an anechoic chamber for measurement.

The simulated radiation efficiency is depicted in Fig. 14. The radiation efficiency is 91.45% at 3.5 GHz and 89.56% at 5.5 GHz.

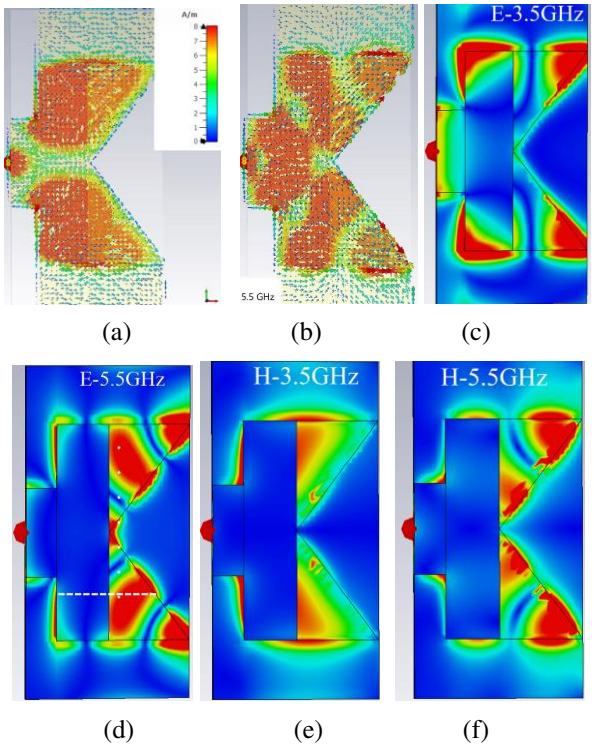

(a) (b) (c)

(d) (e) (f)

Fig. 6. Surface current density, E and H-field contour plot (a) Current at 3.5GHz. (b) Current at 5.5GHz. (c) E-Field at 3.5GHz. (d) E-Field at 5.5GHz. (e) H-Field at 3.5GHz. (f) H-Field at 5.5GHz.

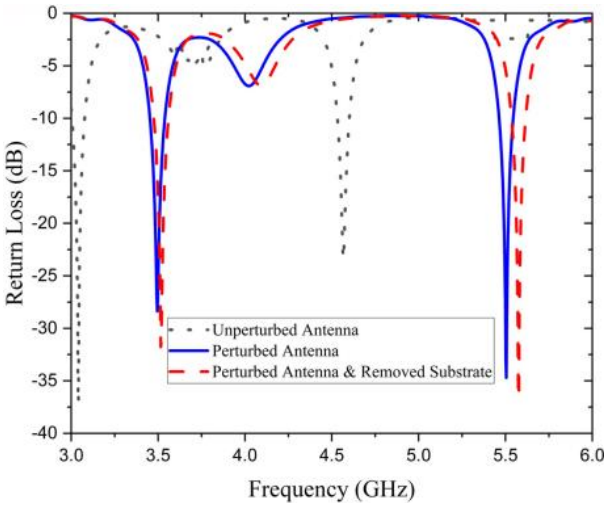

Fig. 7. Resonant frequency shift in three types of the antenna structure.

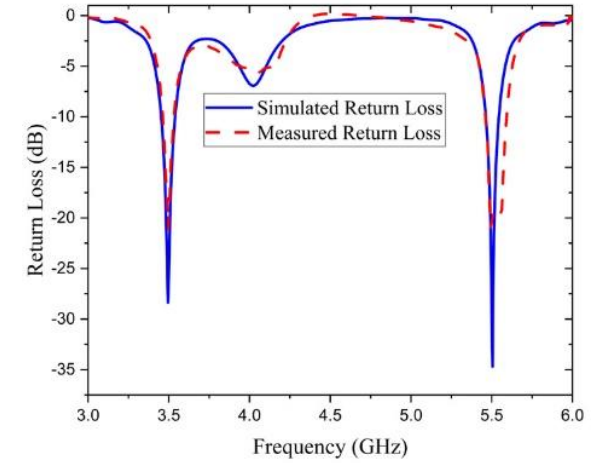

(a)

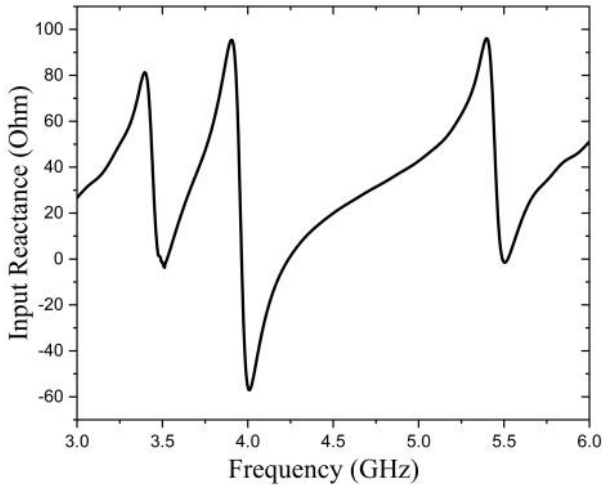

(b)

Fig. 8. (a) Return loss of perturbed antenna. (b) Input reactance.

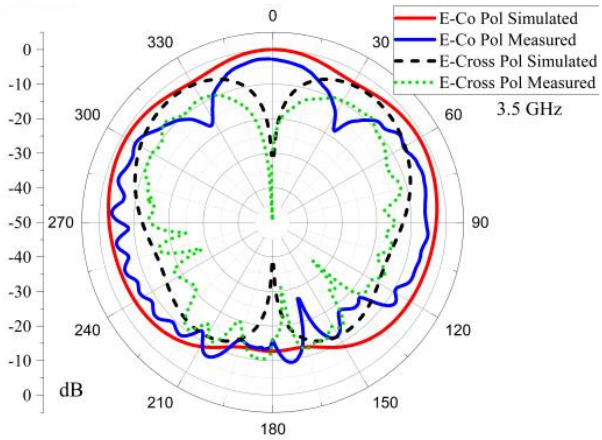

Fig. 9. Co and cross polarization at 3.5GHz for E-plane.

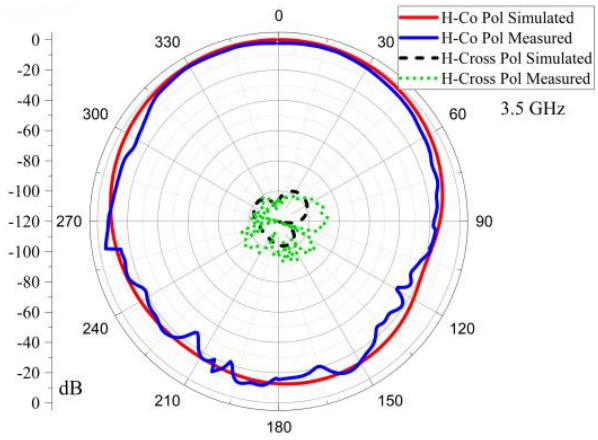

Fig. 10. Co and cross polarization at 3.5GHz for H-plane.

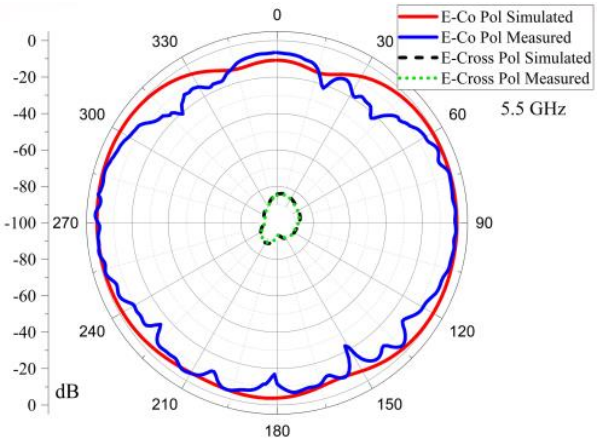

Fig. 11. Co and cross polarization at 5.5GHz for E-plane.

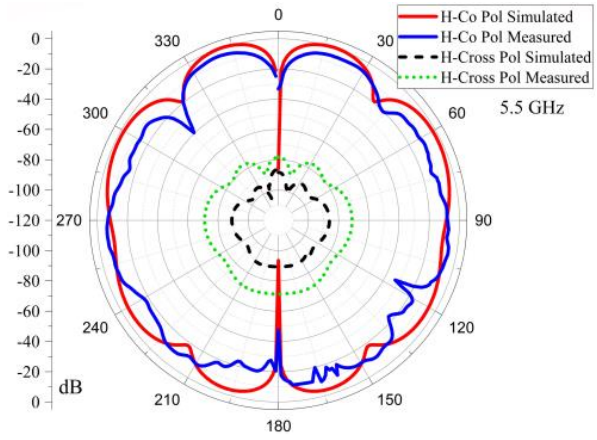

Fig. 12. Co and cross polarization at 5.5GHz for H-plane.

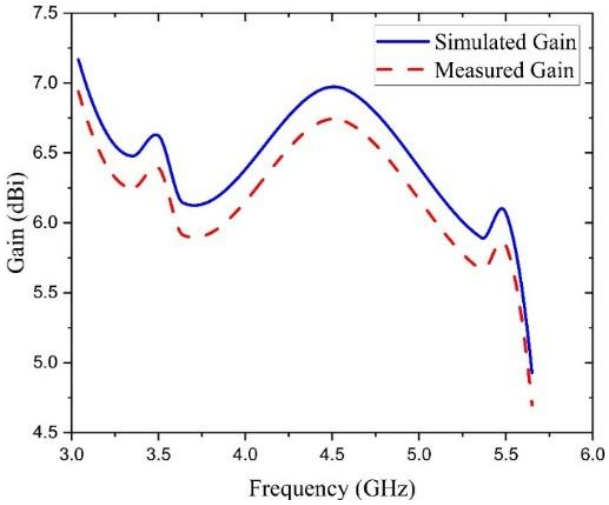

Fig. 13. Simulated and measured gain.

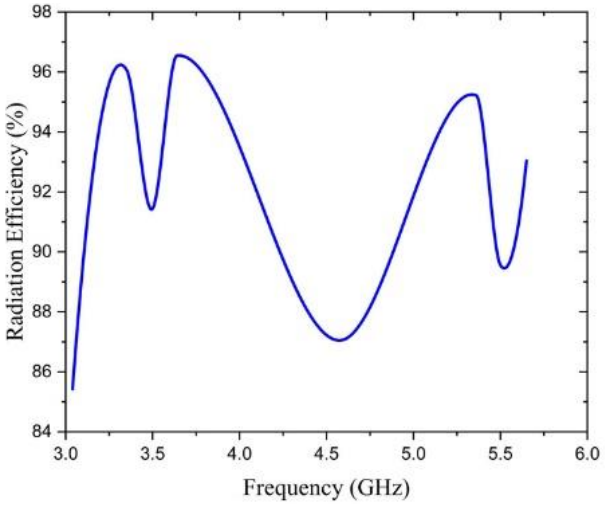

Fig. 14. Simulated Radiation efficiency.

VII. CONCLUSION

A dual-band printed antenna has been designed for WiMAX application. The perturbation technique is applied to study the relationship between the resonant frequency and electromagnetic energy stored in the volume of antenna structure. The result obtained from this technique has been validated with simulation and measurement. The cross-pol level is well below the co-pol. As the structure of this proposed antenna is simple and conformal, it can be printed conveniently on electronic gadgets. The procedure discussed in this article for applying the perturbation technique can be adapted to predict the resonant frequency of any printed antenna loaded with slit or slot or similar patterns from the known resonant frequency of the undisturbed structure. In addition, to study the trend of frequency shift when the antenna's structure is perturbed, numerical methods can be used to compute the energy in the complicated or ununiformed perturbation.

REFERENCES

[1] Z. J. Eleftheriades, "Dual-band metamaterial-inspired small monopole antenna for WiFi applications," *Electron. Lett.,* vol. 45, no. 22, 2009.

[2] X. S. Ren, Y. Z. Yin, W. Hu, and Y. Q. Wei, "Compact tri-band rectangular ring patch antenna with asymmetrical strips for WLAN/WiMax applications," *J. Electromagn. Waves Appl.,* vol. 24, pp. 1829-38, 2010.

[3] B. Yang, Y. Jiao, W. Zhang, H. Xie, and F. Zhang, "Dual-band ring-shaped antenna for WiMAX/WLAN applications," *IEEE Int. Conf. Microw. Technol. Comput. Electromagn.,* pp. 38-40, 2011.

[4] P. Jing, A. G. Wang, S. Gao, and W. Leng, "Miniaturized triple-band antenna with a defected ground plane for WLAN/WiMAX applications," *IEEE Antennas Wirel. Propag. Lett.,* vol. 10, pp. 298-301, 2011.

[5] B. Mazumdar, U. Chakraborty, A. Bhowmik, and S. K. Chowdhury, "Design of compact printed antenna for WiMAX & WLAN applications," *Procedia Technol.*, vol. 4, pp. 87-91, 2012.

[6] H. Zhai, Z. Ma, Y. Han, and C. Liang, "A compact printed antenna for triple-band WLAN/WiMAX applications," *IEEE Antennas Wirel. Propag. Lett.,* vol. 12, pp. 65-8, 2013.

[7] Y. Li and W. Yu, "A miniaturized triple band monopole antenna for WLAN and WiMAX applications," *Int. J. Antennas Propag.*, pp. 1-5, 2015.

[8] R. K. Saraswat and M. Kumar, "Miniaturized slotted ground UWB antenna loaded with metamaterial for WLAN and WiMax applications," *Prog. Electromagn. Res. B.,* vol. 65, pp. 65-80, 2016.

[9] F. Cirik and B. S. Yildirim, "Analysis and design of a 3.5-GHz patch antenna for WiMAX applications," *Int. J. Microw. Wirel. Technol.*, vol. 8, pp. 63-70, 2016.

[10] T. Ali, A. W. M. Saadh, R. C. Biradar, J. Anguera, and A. Andújar, "A miniaturized metamaterial slot antenna for wireless applications," *AEU - Int. J. Electron. Commun.,* vol. 82, pp. 368-82, 2017.

[11] M. Challal, F. Mouhouche, K. Djafri, and A. Boutejdar, "Quad-band microstrip patch antenna for WLAN/WIMAX/C/X applications," *5th Int. Conf. Electr. Eng.,* Boumerdies, Algeria, vol. 1, pp. 1-4, 2017.

[12] T. Ali and R. C. Biradar, "A compact multi-band antenna using $\lambda/4$ rectangular stub loaded with metamaterial for IEEE 802.11N and IEEE

802.16E," *Microw. Opt. Technol. Lett.*, vol. 59, pp. 1000-1006, 2017.

[13] D. Sipal, M. P. Abegaonkar, and S. K. Koul, "Compact planar 3.5/5.5 GHz dual band MIMO USB dongle antenna for WiMAX applications," *IEEE Indian Conf. Antennas Propogation.,* pp. 1-4, 2018.

[14] W. S. Chen, M. H. Liang, T. Y. Zhuo, J. H. Lin, and J. H. Hsu, " Dual-strip monopole antenna for USB dongle applications," *IEEE Int. Work. Electromagn. Student Innov. Compet.,* pp. 1-2, 2018.

[15] P. Osklang, C. Phongcharoenpanich, and P. Akkaraekthalin, "Triband compact printed antenna for 2.4/3.5/5 GHz WLAN/WiMAX applications," *Int. J. Antennas Propag.,* vol. 2019, pp. 1-13, 2019.

[16] N. Ferdous, G. Chin Hock, H. A. S. Hamid, M. N. A. Raman, T. S. Kiong, and M. Ismail, "Design of a small patch antenna at 3.5 GHz for 5G application," *IOP Conf. Ser. Earth Environ. Sci.*, pp. 268, 2019.

[17] X. Li, H. Zhu, and Z. Huang, "A CPW-fed miniaturized dual-band antenna for 5G applications," *IEEE MTT-S Int. Conf. Numer. Electromagn. Multiphysics Model. Optim.,* pp. 1-3, 2020.

[18] O. Benkhadda, S. Ahmad, M. Saih, K. Chaji, A. Reha, A. Ghaffar, S. Khan, M. Alibakhshikenari, and E. Limiti, "Compact broadband antenna with vicsek fractal slots for WLAN and WiMAX applications," *Appl. Sci.*, vol. 12, no. 3, 2022.

[19] S. Tyagi, S. Kanojia, and P. K. Chakarvarti, "Micro strip patch antenna for WLAN/WiMAX applications: a review," *SSRN. Electron. J.*, pp. 162-166, 2020.

[20] P. Sandhiyadevi, V. Baranidharan, G. K. Mohanapriya, J. R. Roy, and M. Nandhini, "Design of dual-band low profile rectangular microstrip patch antenna using FR4 substrate material for wireless applications," *Mater. Today Proc.,* vol. 45, pp. 3506-3511, 2021.

[21] P. Mathur, R. Augustine, M. Gopikrishna, and S. Raman, "Dual MIMO antenna system for 5G mobile phones, 5.2 GHz WLAN, 5.5 GHz WiMAX and 5.8/6 GHz WiFi applications," *IEEE Access.,* vol. 9, pp. 106734-106742, 2021.

[22] K. Mahendran, D. R. Gayathri, and H. Sudarsan, "Design of multi band triangular microstrip patch antenna with triangular split ring resonator for S band, C band and X band applications," *Microprocess Microsyst.,* vol. 80, pp. 103400, 2021.

[23] S. K. Ibrahim and Z. T. Jebur, "A high gain compact rectangular patch antenna for 5G applications," *Int. Conf. Commun. Inf. Technol.*, vol. 2021, pp. 156-160, 2021.

[24] R. Kumar, R. Sinha, A. Choubey, and S. K. Mahto, "A circular monopole antenna with uniquely packed quad T-shaped strips for WLAN/WiMAX application," *Frequenz.,* 2022. https://doi.org/10.1515/freq-2022-0017

[25] A. K. Vallappil, A. M. K. Rahim, A. B. Khawaja, M. N. Iqbal, N. A. Murad, M. M. Gajibo, L. O. Nur, and B. S. Nugroho, "Complementary split-ring resonator and strip-gap based metamaterial fractal antenna with miniature size and enhanced bandwidth for 5G applications," *J. Electromagn. Waves. Appl.,* vol. 36, pp. 787-803, 2022.

[26] S. L. Gunamony, S. Rekha, and B. P. Chandran, "Asymmetric microstrip fed meander line slot antenna for 5.6 GHz applications," *Mater. Today Proc.,* vol. 58, pp. 91-95, 2022.

[27] S. Sharma and D. Kaur, "Measurement of complex permittivity of polystyrene composite at 11.64 GHz using cavity perturbation technique," *Applied Computational Electromagnetics Society (ACES) Journal*, vol. 31, no. 1, pp. 92-97, 2016.

[28] S. Fakhte and H. Oraizi, "Derivation of the resonant frequency of rectangular dielectric resonator antenna by the perturbation theory," *Applied Computational Electromagnetics Society (ACES) Journal*, vol. 31, no. 8, pp. 894-900, 2016.

[29] G. Kumar and K. P. Ray, *Broadband Microstrip Antennas,* Artech House, Boston, London, pp. 33, 2003.

[30] C. A. Balanis, *Antenna Theory Analysis and Design,* 4th ed., John Wiley & Sons, New Jersey, 2016.

[31] R. F. Harrington, *Time-Harmonic Electromagnetic Fields,* 2nd ed., Wiley-IEEE Press, New Jersey, 2001.

[32] S. Pawar and S. Hake, "Effect of different symmetric slits on microstrip patch antenna," *Int. J. Microw. Eng.,* vol. 1, pp. 23-33, 2016.

[33] K. Mondal and P. P. Sarkar, "Gain and bandwidth enhancement of microstrip patch antenna for WiMAX and WLAN applications," *IETE J. Research.,* vol. 67, pp. 726-734, 2021.

[34] R. Sreemathy, S. Hake, S. Sulakhe, and S. Behera, "Slit loaded textile microstrip antennas," *IETE J. Research.,* pp. 1-9, 2020.

[35] E. Baghernia and M. H. Neshati, "Development of a broadband substrate integrated waveguide cavity backed slot antenna using perturbation technique," *Applied Computational Electromagnetics Society (ACES) Journal*, vol. 29, no. 11, pp. 847-855, 2014.

C. Mahendran received the B.E degree in 1997 from Government College of Engineering, Tirunelveli, India and M.E in 2002 from Alagappa Chettiar Government College of Engineering and Technology (ACGCET), Karaikudi, India. He is currently working as an Assistant Professor at ACGCET and is pursuing his Ph.D at Anna University, Chennai, India. He worked as a Scientist (Grade B) in the Broadcast and Communication Group, Centre for Development of Advanced Computing, Thiruvananthapuram, India. His research interests include printed antenna design and RF system design.

M. Vijayaraj received the B.E degree in 1988 from Thiagarajar College of Engineering, Madurai, India and M.E in 1997 from ACGCET, Karaikudi, India. He was awarded a Ph.D from Anna University, Chennai, India in 2010. He is currently working as a Professor in Government College of Engineering, Tirunelveli, India. His research interests include wireless communication and printed antenna design.